Effects of Landfall Location and the Approach Angle of a Cyclone Vortex Encountering a Mesoscale Mountain Range

YUH-LANG LIN

Department of Physics, and Department of Energy & Environmental Systems, and NOAA ISET Center, North Carolina A&T State University, Greensboro, North Carolina

L. CROSBY SAVAGE III

Wind Analytics, WindLogics, Inc., St. Paul, Minnesota

(Manuscript received 3 November 2010, in final form 30 April 2011)

ABSTRACT

The orographic effects of landfall location, approach angle, and their combination on track deflection during the passage of a cyclone vortex over a mesoscale mountain range are investigated using idealized model simulations. For an elongated mesoscale mountain range, the local vorticity generation, driving the cyclone vortex track deflection, is more dominated by vorticity advection upstream of the mountain range, by vorticity stretching over the lee side and its immediate downstream area, and by vorticity advection again far downstream of the mountain as it steers the vortex back to its original direction of movement. The vorticity advection upstream of the mountain range is caused by the flow splitting associated with orographic blocking. It is found that the ideally simulated cyclone vortex tracks compare reasonably well with observed tracks of typhoons over Taiwan's Central Mountain Range (CMR).

In analyzing the relative vorticity budget, the authors found that jumps in the vortex path are largely governed by stretching on the lee side of the mountain. Based on the vorticity equation, this stretching occurs where fluid columns descend the lee slope so that the rate of stretching is governed mostly by the flow speed and the terrain slope. In other words, the maximum stretching and associated track jump are located on the faster side of the vortex. In the type E and N landfalling tracks, the faster winds are well north of the mountain crest, and the vortex track has very little change across the mountain. For the S case, however, the stronger winds are near the center of the ridge, and the track jump is much larger. For the NE case, the jump in the vortex track occurs once the vortex center shifts south of the ridge. For the SE case, there is considerable stretching, but it is aligned with the original track, so there is no jump in track.

1. Introduction

As a tropical cyclone (TC) passes over a mesoscale mountain range, its track is often deflected (Lin et al. 1999), as occurs with typhoons passing over the Central Mountain Range (CMR) of Taiwan, the Cordillera Central of northern Luzon in the Philippines (Wang 1980; Bender et al. 1987), or with hurricanes passing over the southern Appalachian Mountains (O'Handley and Bosart 1996), the Cordillera Central of Hispañola (Bender et al. 1987) and the Sierra Madre of Mexico (Zehnder 1993; Zehnder and Reeder 1997). Similar deflections have also been observed with midlatitude cyclones passing over the Appalachians (O'Handley and Bosart 1996) and the mountains in Greenland (Schwierz and Davies 2003). Because it is a steep mountain range isolated by significant bodies of water and is often traversed by western Pacific TCs, the CMR has been studied extensively for its orographic influence on TC track continuity and deflection (e.g., Wang 1980; Chang 1982; Yeh and Elsberry 1993a,b; Lin et al. 1999, 2005).

Lin et al. (2005) identified six prospective nondimensional control parameters for diagnosing the continuity and deflection of cyclone tracks across a mesoscale mountain range. From previous studies (e.g., Wang 1980; Chang 1982; Yeh and Elsberry 1993a,b; Lin et al. 2005; Lin 2007; also see Fig. 1) of observed and simulated typhoons

Corresponding author address: Prof. Yuh-Lang Lin, 101 Marteena Hall, Department of Physics, North Carolina A&T State University, 1601 E. Market St., Greensboro, NC 27411.
E-mail: ylin@ncat.edu.

DOI: 10.1175/2011JAS3720.1

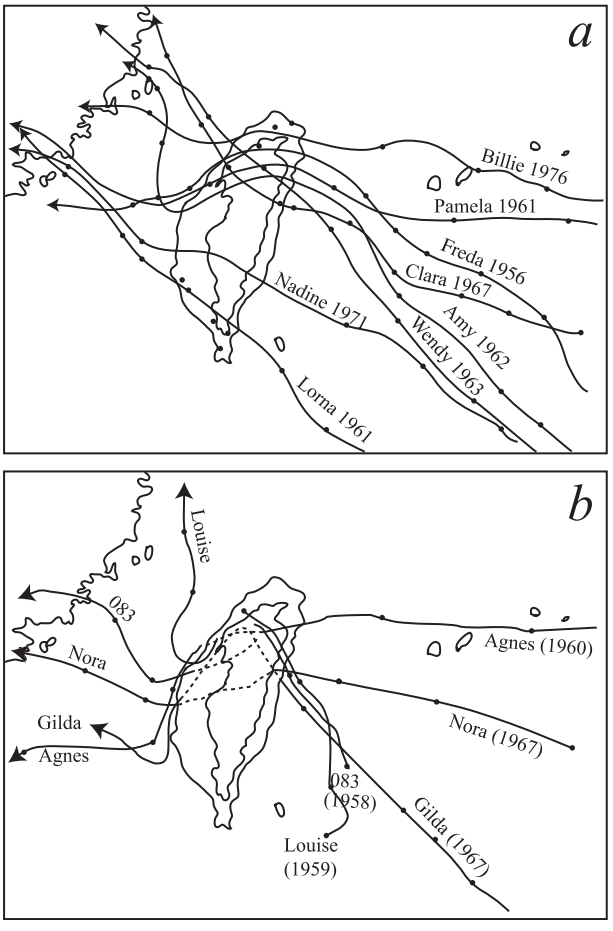

FIG. 1. Typhoons traversing the Central Mountain Range (CMR) of Taiwan with (a) continuous and (b) discontinuous tracks. [Adapted from Wang (1980), Chang (1982), and Lin et al. (2005)].

traversing the CMR, it has been found that the cyclone track is discontinuous (continuous), and the cyclone encounters more (less) deflection in its motion, with a combination of small (large) values of the parameters $V_{\max}/Nh$, U/Nh, R/L_y, U/fL_x, and $V_{\max}/fR$, and a large (small) value of the parameter h/L_x. Here $V_{\max}$ is the maximum tangential wind; N, the Brunt–Väisäla frequency; h, the mountain height; U, the basic wind speed; R, the radius of $V_{\max}$; f, the Coriolis parameter; and L_x and L_y, the horizontal scales of the mountain in the x and y directions, respectively. In particular, the first three parameters were found to play a dominant role in controlling the deflection of cyclone tracks for typhoons passing over an idealized CMR. The left or right track deflection appears to be controlled more dominantly by $V_{\max}/Nh$ and R/L_y, while the degree of track deflection is controlled more dominantly by U/Nh. In general, track deflection is controlled by the fundamental dynamics of *orographic blocking*.

In addition to the above-listed control parameters, the deflection in the track of a tropical cyclone traversing the CMR is also strongly influenced by landfall location and approach angle (e.g., Wang 1980; Chang 1982; Yeh and Elsberry 1993a,b). In this study, we examine the fundamental dynamics of the track deflection influenced by these two factors by performing idealized numerical simulations with a drifting cyclone vortex passing over topography representative of the CMR. The numerical model and its experimental design are described in section 2, while the results and their applications to real cases of typhoons passing over Taiwan's CMR are discussed in section 3. The fundamental dynamics associated with vorticity budget analysis are also presented. Concluding remarks are made in section 4.

2. Model description and experiment design

We employ a mesoscale numerical model, the Geophysical Fluid Dynamics Model (GFDM), see Lin et al. 1999), to understand the dynamics involved with different landfall locations and approach angles that affect the track of a cyclone over an idealized mesoscale mountain range. The model has been adopted in previous studies for idealized simulations of tropical cyclones passing over mesoscale mountain ranges (e.g., Lin et al. 1999, 2005) as well as other fundamental studies on flow regimes and gravity waves associated with stratified fluid flow over mountains (e.g., Lin and Wang 1996; Shen and Lin 1999; Wang and Lin 1999).

The major characteristics of the model are summarized as follows:

- the time-dependent, hydrostatic governing equations solved on an Arakawa-C staggered grid;
- the third-order Adams–Bashforth scheme used for time marching;
- the horizontal (vertical) advection terms approximated using a quadratic conservative fourth (second)-order centered finite difference;
- a terrain-following σ_z vertical coordinate adopted (Lin and Wang 1996), where σ is defined as $\sigma = z_T(z - h)/(z_T - h)$ in which z_T and h are the heights of the computational domain and terrain elevation, respectively;
- a free-slip lower-boundary condition;
- a radiation upper-boundary condition;
- the horizontal average of pressure at the top of the domain subtracted from the pressure field everywhere to reduce truncation errors (Gary 1973; Clark 1977); and
- a five-point numerical smoother used for diffusion.

Details of the numerical formulation of the model can be found in Lin et al. (1999).

For the cases presented here, a uniform, stably stratified basic flow is introduced instantaneously and throughout the grid domain at nondimensional time $t = 0$. The Brunt–Väisälä frequency is set as $N = 0.01\ \mathrm{s}^{-1}$ for all experiments performed in this study. An *f*-plane approximation has also been made, where the Coriolis parameter f_o is taken to be $5.8 \times 10^{-5}\ \mathrm{s}^{-1}$ corresponding to that at latitude 23.5°N, which crosses central Taiwan. The flow is inviscid throughout the entire model domain. The vertical grid interval is 500 m, while the horizontal grid interval is $\Delta x = \Delta y = 20$ km. The numbers of grid points over the x, y, and z axes are $101 \times 81 \times 31$ for a domain size of 2000 km × 1600 km × 15 km. The CMR is idealized by a bell-shaped function as

$$h(x, y) = \frac{h}{[(x/a)^2 + (y/b)^2 + 1]^{3/2}}, \qquad (1)$$

where h is the mountain height and a and b are the mountain half-widths in the x and y directions, respectively. For all cases performed in this study, we use $h = 2.5$ km, $a = 40$ km, and $b = 120$ km, which are values comparable to those attributed to the CMR. Note that we use $2a$ and $2b$ to roughly represent the horizontal scales of the mountain L_x and L_y, respectively.

Following Lin et al. (2005), an idealized tropical cyclone is initialized with a prescribed tangential velocity following Chang (1982) and Huang and Lin (1997):

$$V_\theta = V_{\max}\left(\frac{r}{R_{\max}}\right)\exp\left\{\frac{1}{2}\left[1 - \left(\frac{r}{R_{\max}}\right)^2\right]\right\}, \qquad (2)$$

$V_{\max}$ is the maximum tangential velocity at a radius of $R_{\max}$ from the cyclone vortex center. The initial vortex is assumed to be in gradient wind balance and nondivergent. The $R_{\max}$ is assumed to be 180 km, as in Lin et al. (1999, 2005), and the vertical profile of $V_{\max}$ is $20\ \mathrm{m\ s}^{-1}$ under 4.5 km, decreases approximately linearly to $-10\ \mathrm{m\ s}^{-1}$ at 9 km, and increases to $0\ \mathrm{m\ s}^{-1}$ at 11 km and above. As mentioned in earlier papers of Lin et al. (1999, 2005), a relative larger cyclone vortex is adopted to keep the vortex stable owing to the lack of latent heating. The details of the model initialization procedure can be found in Lin et al. (1999). As latent heating effects were not used in this study, simulated cyclone vortices were prescribed with relatively large radii of the maximum wind R to ensure barotropic stability with the simulated vortex.

This problem is studied by performing systematic numerical modeling simulations using the aforementioned GFDM mesoscale model. The nondimensional control parameters are fixed with $U/Nh = 0.4$, $V_{\max}/Nh = 0.8$, and $R/L_y = 0.75$, which correspond to the following dimensional parameters: $U = 10\ \mathrm{m\ s}^{-1}$, $N = 0.01\ \mathrm{s}^{-1}$, $h = 2.5$ km, $f = 5.8 \times 10^{-5}\ \mathrm{s}^{-1}$, $V_{\max} = 20\ \mathrm{m\ s}^{-1}$, $R = 180$ km, $a = 40$ km, $b = 120$ km, and $L_y = 2b = 240$ km. This setting belongs to a moderate blocking case, such as case B2 of Lin et al. (2005).

The control case (case E) has the cyclone vortex approaching the idealized mountain range from a point 500 km east of the mountain range center (i.e., the idealized CMR), or from $(x/a, y/a) = (12.5, 0.0)$. The *effect of landfall location* is then studied through two additional cases: 1) case N in which the cyclone vortex is approaching the mountain range from the east toward the west starting with $(x/a, y/a) = (12.5, 2.25)$; and 2) case S in which the cyclone approaching from the east is toward the west starting with $(x/a, y/a) = (12.5, -2.25)$.

The *effect of approach angle* is studied through two more cases, bothin which the cyclone vortex encounters the mountain range at an east-central location with $(x/a, y/a) = (1.0, 0.0)$. In case NE the cyclone vortex approaches the mountain range starting from a northeast point with $(x/a, y/a) = (8.133, 8.132)$; in case SE the cyclone vortex approaches the mountain range from a southeast point with $(x/a, y/a) = (8.133, -8.132)$.

The *effects of both approach angle and landfall location* are studied through four additional cases, all in which encounter the mountain range at a northeast location with $(x/a, y/a) = (0.0, 2.25)$ or a southeast location with $(x/a, y/a) = (0.0, -2.25)$. In case NE-N the cyclone vortex approaches from $(x/a, y/a) = (8.133, 10.381)$ and encounters the northern mountain range at $(x/a, y/a) = (0.0, 2.25)$; in case NE-S the cyclone vortex approaches from the northeast at $(x/a, y/a) = (8.133, 5.881)$ and encounters the southern mountain range at $(x/a, y/a) = (0.0, -2.25)$. Case SE-S approaches the mountain range from the southeast at $(x/a, y/a) = (8.133, -10.381)$ and encounters the southern mountain range at $(x/a, y/a) = (0.0, -2.25)$, while case SE-N approaches the mountain range from the southeast at $(x/a, y/a) = (8.133, -5.881)$ and encounters the northern mountain range at $(x/a, y/a) = (0.0, 2.25)$.

These experiments are summarized in Table 1.

3. Results

a. Effects of landfall location

Figure 2a shows the tracks of the cyclone vortex centers at the surface and 500 mb for case E (track type E). At the surface, the cyclone is *deflected slightly to the north* before it encounters the mountain*, slightly to the south* as it is crossing over the mountain, and *to the north*

TABLE 1. Summary of numerical experiments. The control parameters are fixed with $U/Nh = 0.4$, $V_{max}/Nh = 0.8$, and $R/L_y = 0.75$. The corresponding dimensional values of the parameters are $U = 10$ m s^{-1}, $N = 0.01$ s^{-1}, $h = 2.5$ km, $f = 5.8 \times 10^{-5}$ s^{-1}, $V_{max} = 20$ m s^{-1}, $R = 180$ km, $a = 40$ km, $b = 120$ km, and $L_y = 2b = 240$ km.

Case	Starting location (x/a, y/a)	Landfall location (x/a, y/a)	Effects studied
E	500 km from east (12.5, 0.0)	East-central CMR (1.0, 0.0)	Landfall location
N	500 km from east (12.5, 2.25)	Northeast CMR (0.0, 2.25)	Landfall location
S	500 km from east (12.5, −2.25)	Southeast CMR (0.0, −2.25)	Landfall location
NE	Northeast (8.133, 8.132)	East-central CMR (1.0, 0.0)	Approach angle
SE	Northeast (8.133, −8.132)	East-central CMR (1.0, 0.0)	Approach angle
NE-N	Northeast (8.133, 10.381)	Northeast CMR (0.0, 2.25)	Landfall location and approach angle
NE-S	Northeast (8.133, 5.881)	Southeast CMR (0.0, −2.25)	Landfall location and approach angle
SE-S	Southeast (8.133, −10.381)	Southeast CMR (0.0, −2.25)	Landfall location and approach angle
SE-N	Southeast (8.133, −5.881)	Northeast CMR (0.0, 2.25)	Landfall location and approach angle

after crossing the mountain, and then *resumes to its original westward movement* far downstream (to the west) of the mountain. The track is *less affected* by the mountain at 500 mb, as denoted by a gray curve in Fig. 2a. The surface relative vorticity fields at $t = 9$, 12, 15, and 18 h are shown in Figs. 3a–d. At $t = 9$ h (Fig. 3a), the vortex center is located at about (x/a, y/a) = (10.0, 0.0), indicative of no deflection in cyclone motion. A weak vortex center forms on the lee side at this time. Before the cyclone encounters the mountain at $t = 12$ h (Fig. 3b), the upstream vorticity pattern is distorted slightly north and the track of the vortex center is deflected to the north as well. At 15 h (Fig. 3c), the lee side vortex center becomes the cyclone center, with a resulting discontinuity in the track (Fig. 2a). At 18 h (Fig. 3d), the cyclone is deflected to the north and resumes its original westward motion.

The track deflection belongs to the moderate blocking case of the conceptual model for moderate blocking proposed by Lin et al. (2005) (see Fig. 4b). In fact, the ideally simulated track of the cyclone vortex approaching the central portion of the mountain range from the east (track type E) compares reasonably well with the observed track of Typhoon Nora (1967) as analyzed by Wang (1980) and presented in Fig. 1b. Other examples of track type E are Typhoons Elsie (1966–11), Nina (1975–04), Omar (1992–15), and Longwang (2005–19) (Table 2, tracks not shown), based on the tracks analyzed by Shieh et al. (1998) and Digital Typhoon (2011). Note that the observed typhoon tracks are analyzed in more detail by Shieh et al. compared to those shown in Digital Typhoon. Most of these typhoons exhibit similar tracks as simulated, except Nina and Elsie, which turned to the south upstream of the CMR. This may be explained by stronger orographic blocking resulting in a track deflection more representative of the conceptual model shown in Fig. 4c.

Deflection to the surface track of the cyclone approaching from the east can be explained through a vorticity budget analysis, in which individual terms of the vorticity equation,

$$\frac{\partial \zeta}{\partial t} = -\mathbf{V} \cdot \nabla \zeta - (\zeta + f_0)\left(\frac{\partial u}{\partial x} + \frac{\partial v}{\partial y}\right) + \left(\xi \frac{\partial w}{\partial x} + \eta \frac{\partial w}{\partial y}\right) + R, \tag{3}$$

are calculated. In Eq. (3) ξ, η, and ζ represent vorticity in the x, y, and z directions, respectively. The term on the left side is the local rate of change of the vertical relative vorticity or local vorticity generation. The terms on the right side represent, from left to right, vorticity advection, vorticity stretching, vorticity tilting, and the combined effects of turbulent mixing and numerical diffusion. Since the fluid is assumed to be Boussinesq, no solenoidal term is included in the vorticity equation. Figure 5a shows the local rate of change of the vertical vorticity at 9 h. The major area for local vorticity generation is located to the southwest of the mountain range, and a minor area is located near the eastern edge of the mountain range (Fig. 5a), mainly as a product of vorticity advection with slight enhancement by vorticity stretching for the lee-side maximum area (Figs. 5b and 4c). Since the upstream local vorticity generation maximum is centered at $y/a = 0$, the track of the vortex center runs straight westward.

At 12 h (Fig. 6), the maximum area of local vorticity generation is located over the lee side, which is a result of vorticity stretching to the west and of vorticity advection to the southwest. At this time the maximum of vorticity advection (Fig. 6b) is still located upstream of the mountain range. The vortex center is located slightly to the north of the $y/a = 0$ line, indicative of a slight northward deflection in the vorticity track. Figure 6c indicates that the vorticity over the lee side and its immediate downstream area is dominated by stretching. Apparently, this stretching occurs where fluid columns descend the lee slope so that the rate of stretching is governed mostly by the flow speed and the terrain slope.

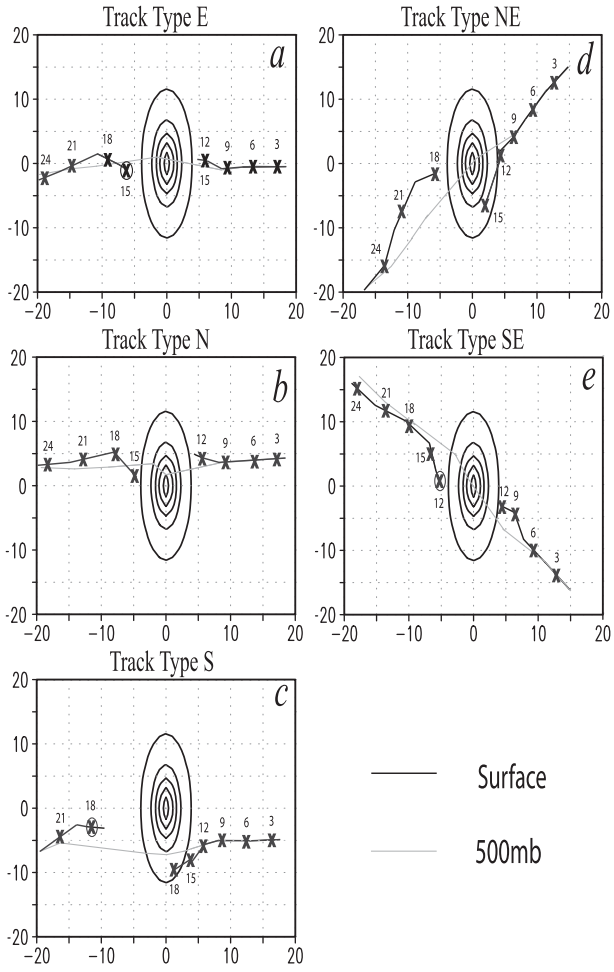

FIG. 2. GFDM simulated tracks of cyclone vortex centers from the east, north, south, northeast, and southeast (track types E, N, S, NE, and SE, respectively) near the surface (dark curve) and 500 mb (gray curve). The crosses denote 3-hourly surface positions. A circled cross denotes a second, coexisting vortex center. Thick ovals denote terrain at every 400 m. Area shown is 800 km × 800 km.

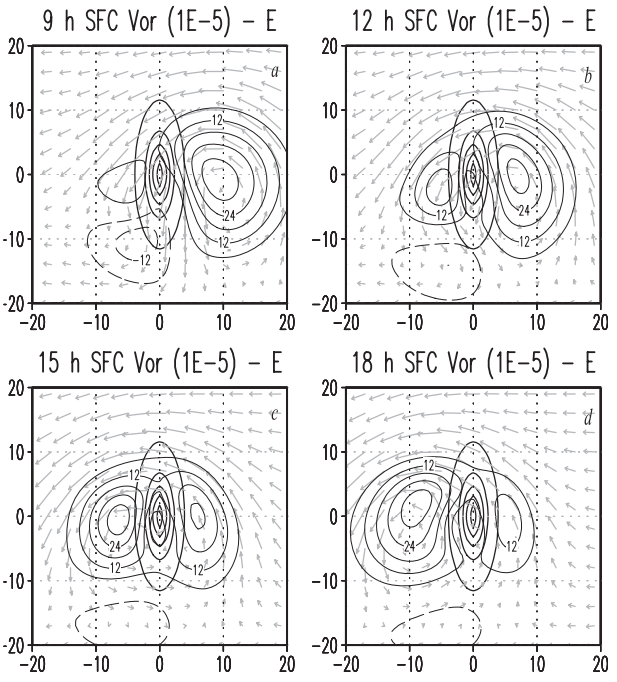

FIG. 3. GFDM simulated relative vorticity and wind vectors for case E near the surface at 9, 12, 15, and 18 h. Vorticity is contoured every 6×10^{-5} s^{-1}. Solid (dashed) lines are positive (negative) values.

This can be shown as follows. Based on Eq. (3), the local generation of relative vorticity can be expressed by

$$\frac{\partial \zeta}{\partial t} \propto -(\zeta + f_0)\left(\frac{\partial u}{\partial x} + \frac{\partial v}{\partial y}\right) = (\zeta + f_0)\frac{\partial w}{\partial z}. \qquad (4)$$

Since the vertical motion w across the mountain is governed by the flow speed and mountain slope (i.e., $U\,\partial h/\partial x$), maximum stretching would occur where the fastest wind is located. Since the vortex itself is very asymmetric, with fast winds on the lee side and weaker winds on the upstream side (Figs. 5–8), the maximum stretching and associated jump in track occurs when the vortex is located over the center of the mountain range. For the current case, the stronger wind is well north of the mountain crest; thus the vortex track has very little change across the mountain in terms of the north–south deflection as the vortex ''jumps'' over the mountain. After the vortex jumps over the mountain (Figs. 7 and 8), the vortex track is steered primarily by vorticity advection. Note that vorticity tilting plays a minor role in the process of track deflection, as shown in Figs. 6d, 7d, and 8d.

Figure 9 shows the vorticity fields at $t = 9$, 12, 15, and 18 h for case N (track type N). The vortex center is *deflected slightly northward* of its original east–west track *before encountering* the mountain range. The cyclone vortex is *deflected to the south* during its passage *over* the mountain range, *to the north* on the lee side of the mountain range, and then *resumes westward movement far downstream* (Fig. 2b). Based on the vorticity budget analysis (not shown), the slight upstream northward deflection is due to vorticity advection, while the southward deflection during its passage over the mountain is dominated by the vorticity stretching. The resumption of westward motion is controlled by vorticity advection. Similar to case E, the faster winds are well north of the mountain crest, and the vortex track has very little change across the mountain in terms of north–south locations of the vortex jump over the mountain.

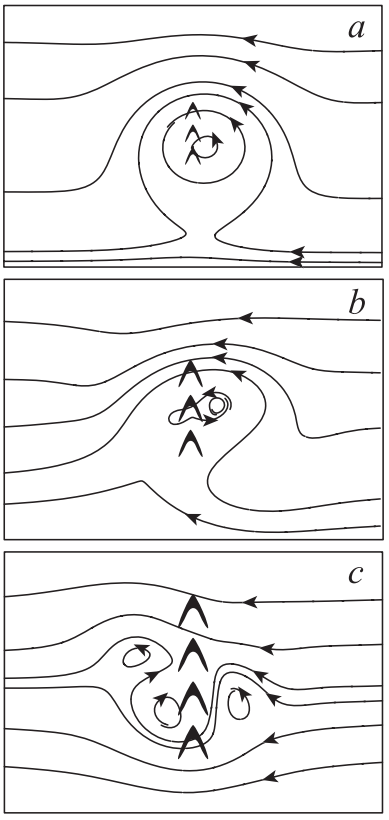

FIG. 4. Conceptual model depicting three different responses of the westward-moving cyclone to orographic forcing. (a) Weak blocking: the cyclone is deflected slightly northward upstream of the mountain range but follows a continuous cyclone track. (b) Moderate blocking: the cyclone is deflected northward upstream of the mountain range, while a secondary vortex forms to the southwest of the mountain range, leading to a discontinuous cyclone track. (c) Strong blocking: the behavior of the cyclone is similar to (b) except the cyclone is deflected to the south and a secondary cyclone is generated at the northwestern slope of the mountain range, resulting in a discontinuous track for the cyclone. [Adapted from Lin et al. (2005) and Lin (2007).]

The observed tracks of Typhoons Pamela (1961) and Billie (1976) (Fig. 1a) possess similar behavior of the ideally simulated track type N. Note that the tracks of Pamela and Billie are continuous, indicating that the orographic blocking is weak or at most moderate (Fig. 4a). Other examples of track type N include Typhoons Salby (1960), Norris (1980), Yancy (1990), and Herb (1996) (Table 2, tracks not shown).

Figure 10 shows the vorticity fields at $t = 9, 12, 15$, and 18 h for case S (track type S). The vortex center curves clockwise around the southern part of the mountain range, overshoots to the north on the lee side, and then resumes westward movement far downstream (Fig. 2c). Based on the vorticity budget analysis (not shown), the upstream southward deflection is due to vorticity advection as the cyclone approaches the mountain. Around $t = 15$ h, the northward deflection on the lee side is dominated by vorticity stretching. Far downstream from the mountain range, the cyclone vortex resumes westward movement due to vorticity advection. Unlike the E and N cases, the stronger winds are near the center of the ridge, and the track jump is much larger. A *track jump* is defined loosely as a large deflection of the cyclone vortex in the direction perpendicular to the original track without mountain.

Tracks of Tropical Storm B70 (1914) and Typhoons Sally (1961) and Betty (1975) (Shieh et al. 1998; not shown), although continuous, are similar to the ideally simulated track type S (Fig. 2c). Typhoon Dot (1982) (see Digital Typhoon 2011), also belongs to track type S but with a less pronounced southward deflection upstream of the CMR as the ideally simulated track. However, the northward jump of the track on the lee side is consistent with the numerical result.

b. *Effects of approach angle*

For cyclone landfall at the east-central part of the mountain range from the northeast (case NE, track type NE) the surface vortex center deviates slightly to the left (south) due to vorticity advection; it then deviates to the right after passing the peak of the mountain range (Figs. 2d and 11). The vortex center then turns cyclonically and resumes southwestward movement far downstream. At $t = 9$ h, a region of strong vorticity advection is produced over the northern portion of the mountain, mainly due to the flow splitting at the east-central landfall location. This vorticity advection helps to advect the vortex center to the northeast of the mountain upstream. Note that the northerly jet used by Lin et al. (1999) and Jian and Wu (2008) to explain the upstream southward deflection, or looping, of typhoons impinging on CMR is associated with this flow splitting under strong orographic blocking (Fig. 4c), as explained in Lin et al. (2005).

The strong northeasterly wind over the lee slope tends to produce strong positive vorticity stretching. At $t = 12$ h, the vorticity stretching strengthens, causing the vortex to split with one center located to the northeast of the mountain and a new one developed on the lee side of the mountain (Fig. 11b). Around $t = 15$ h, the local rate of change of vorticity is dominated by the vorticity stretching term, which has a maximum over the west-central portion of the mountain range. The vortex center is therefore deflected to the right on the lee side near the mountain (Fig. 2d). At $t = 18$ h, the vortex resumes its original southwestward movement, which is controlled by vorticity advection.

TABLE 2. Summary of observed typhoon tracks over the Central Mountain Range (CMR) of Taiwan [based on Shieh et al. (1998) and Digital Typhoon (2011)].

Track type	Typhoon names [based on Shieh et al. (1998) and Digital Typhoon (2011)]
E	Nora (1967), Elsie (1969), Nina (1975), Omar (1992), Longwang (2005)
N	Salby (1960), Pamela (1961), Billie (1976), Norris (1980), Yancy (1990), Herb (1996)
S	TS B70 (1914), Sally (1961), Betty (1975), Dot (1982)
NE	Fanapi (2010)
SE	Iris (1955), Joan (1959), Gilda (1967), Nadine (1971), Andy (1982), Caitlin (1994), Tim (1994), Amber (1997), Toraji (2001), Fung-Wong (2008)
NE-N	Agnes (1960), Nari (2001)
NE-S	Bopha (2006)
SE-N	Dinah (1956), Freda (1956), TS 083 (1958), Louise (1959), Betty (1961), Opel (1962), Amy (1962), Alex (1984), Jangmi (2008)
SE-S	Gilda (1956), Lorna (1961), Andy (1982), Dot (1982)

Track type NE is much less frequently observed, compared to other types of tracks, because most of the typhoons originate from the southeast and east. One example of track type NE is Typhoon Fanapi (2010) [track not shown but can be found in Digital Typhoon (2011)] deviated to the south along the eastern flank of CMR and reformed at a location to the south of the landfall point, consistent with the ideally simulated track type NE (Fig. 2d).

For cyclone landfall from the southeast (case SE), the track deflection of the surface cyclone vortex center is quite different from track type NE (Figs. 2e and 12). The vortex center is deflected to the right (left) upstream (downstream) of the mountain peak but resumes its northwestward movement far downstream. The rightward deflection of the vortex center upstream is mainly due to vorticity advection, while the leftward deflection downstream is influenced mainly by vorticity stretching.

Track type SE is the most commonly observed track for typhoons passing over Taiwan's CMR. One example is Typhoon Gilda (1967), which has a discontinuous track (Fig. 1b) similar to the ideally simulated track type SE (Fig. 2e). Another example is Typhoon Nadine (1971), though with a continuous track (Fig. 1a). Other examples include Andy (1982), Joan (1959), Caitlin (1994), Iris (1955), Tim (1994), Amber (1997), Toraji (2001), and Fung-Wong (2008). All of their tracks (Digital Typhoon 2011; Shieh et al. 1998) are similar to track type SE.

c. *Effects of landfall location and approach angle*

Figure 13a shows the vorticity tracks of case NE-N, which is affected by the mountain upstream causing a deflection to the left (south). This leftward deflection is mainly influenced by vorticity stretching. At $t = 18$ h, the flow splits with two regions of maximum vorticity oriented northwest and southeast around the mountain range. The split flow is caused by an increase in vorticity stretching on the lee side of the mountain, and at $t = 21$ h the lee-side vorticity stretching becomes dominant, creating a rightward deflection. At $t = 27$ h, vorticity advection controls the cyclone, which resumes its southwestward movement. The simulated track type NE-N is consistent with the observed track of Typhoon Agnes (1960), as shown in Fig. 1b. This type of track is also similar to track type NE, such as Typhoon Louise (1959) and Tropical Storm 083 (1958) (Fig. 1b).

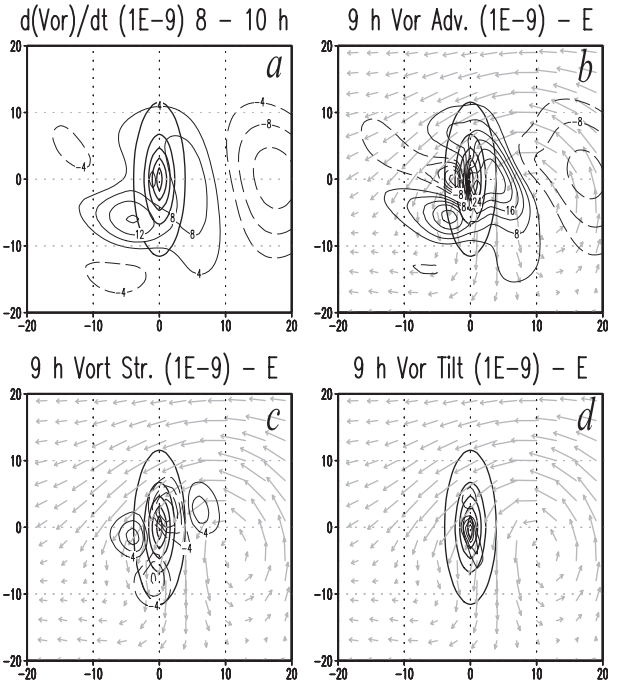

FIG. 5. GFDM simulated vorticity budget and wind vectors at 9 h for case E. Terms shown are local rate of change of relative vorticity, vorticity advection, vorticity stretching, and vorticity tilting. Contours are plotted every 4×10^{-9} s^{-2} except advection is plotted every 6×10^{-9} s^{-2}.

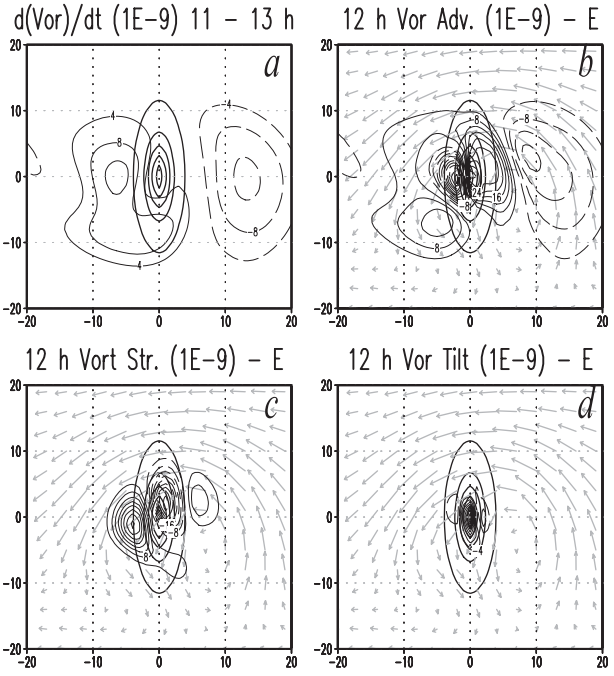

FIG. 6. As in Fig. 5 (case E), but at 12 h.

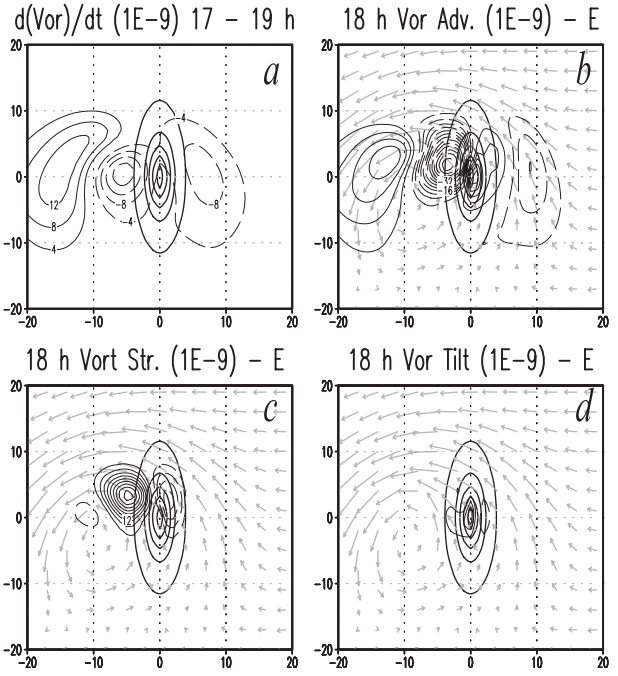

FIG. 8. As in Fig. 5 (case E), but at 18 h.

For cyclone landfall at the southern part of the mountain range from the northeast (case NE-S), the vortex center again follows a similar path to track type NE. Just like track type NE, a region of strong vorticity advection forms near the east-central part of the mountain and is enhanced by a north–south dipole configuration of vorticity stretching. Again a dipole pattern of local vorticity cancels any influence on cyclone motion. At $t = 15$ h, the vortex center is deflected to the right on the lee side near the mountain owing to an increase in vorticity stretching

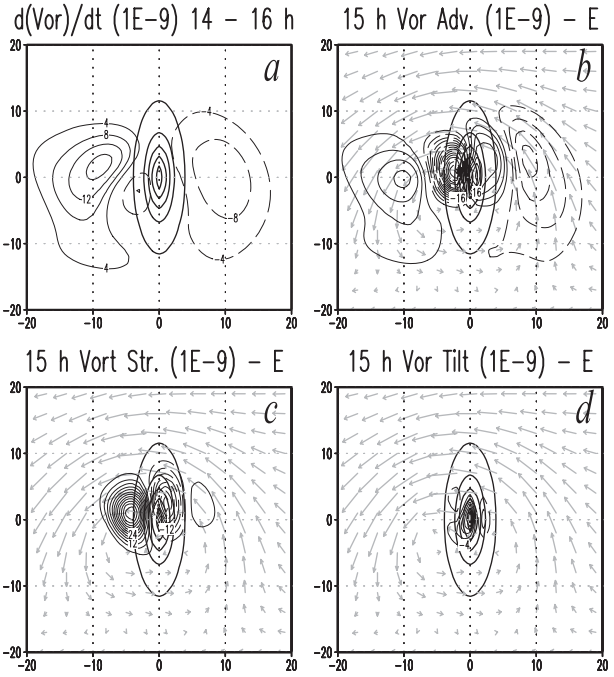

FIG. 7. As in Fig. 5 (case E), but at 15 h.

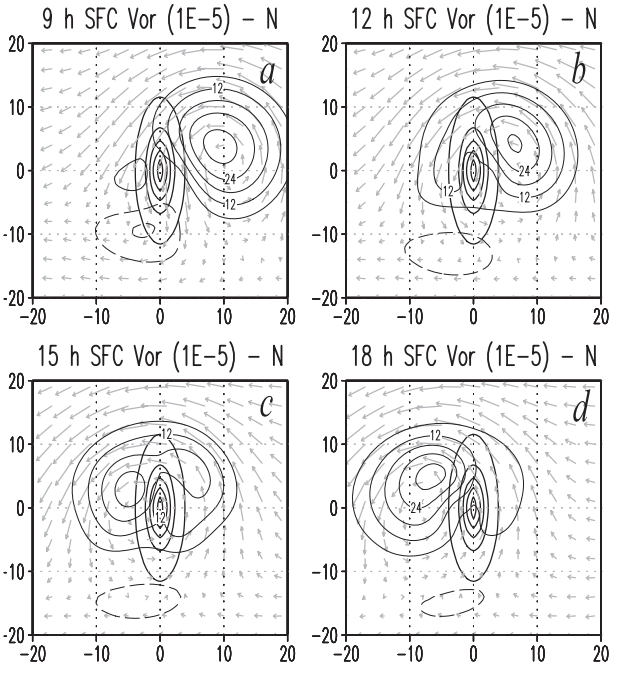

FIG. 9. As in Fig. 3 (GFDM-simulated relative vorticity near the surface at 9, 12, 15, and 18 h), but for case N.

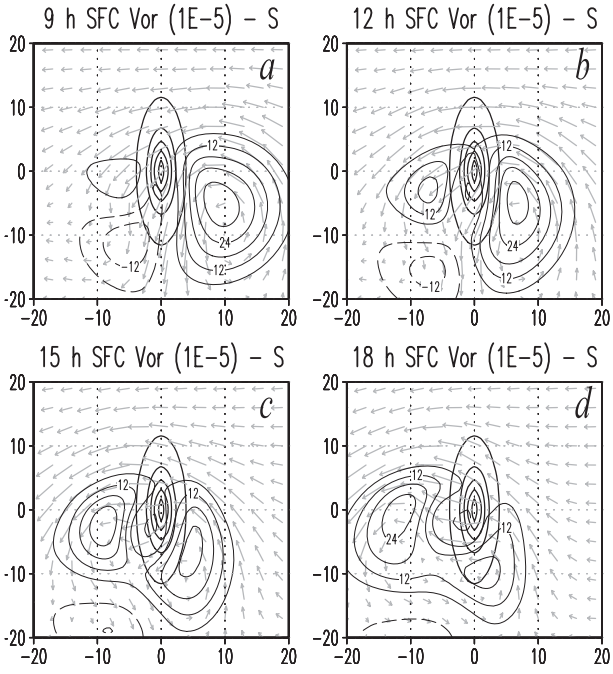

FIG. 10. As in Fig. 9, but for case S.

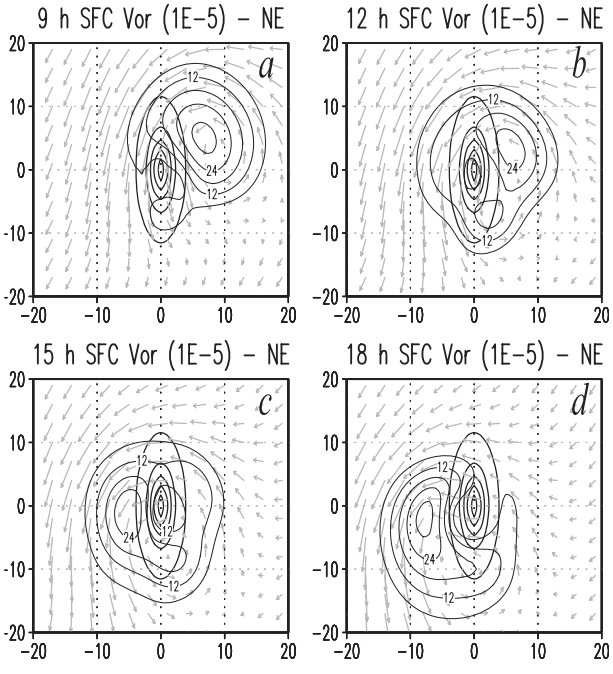

FIG. 11. As in Fig. 9, but for case NE.

(Fig. 13b). The cyclone then returns to its original track as vorticity advection takes control. One example of track type NE-S is Typhoon Bopha (2006) [track not shown, but can be found in Digital Typhoon (2011)], which followed a track similar to that in Fig. 13b.

For cyclone landfall at the northern portion of the mountain range from the southeast (case SE-N), the vortex center follows a path similar to track type SE. Upstream of the mountain the center is deflected to the right by vorticity advection (Fig. 13c). At $t = 12$ h, a second vortex center develops on the lee side from vorticity stretching and has a leftward deflection. This vorticity maximum becomes dominant at $t = 15$ h and moves directly northward owing to both vorticity stretching and advection. The cyclone then resumes its original track and is mainly controlled by vorticity advection.

Similar to track type SE, there are abundant examples of track type SE-N. Examples of track type SE-N can be found in Fig. 1b, such as Typhoon Louise (1959) and Tropical Storm 083 (1958). The ideally simulated track and the real tracks compare reasonably well. Other examples of track type SE-N are Dinah (1956), Freda (1956), Amy (1962), Betty (1961), Opel (1962), Alex (1984), and Jangmi (2008) (Digital Typhoon 2011; Shieh et al. 1998).

Figure 13d shows the cyclone vortex track of case SE-S. Upstream of the mountain range the cyclone is deflected to the left by a region of strong vorticity advection. At $t = 12$ h, the flow splits into two regions of maximum vorticity: one center is located to the south of the mountain and the other is located to the west of the mountain. The southern center of maximum vorticity is controlled by vorticity advection, while the western

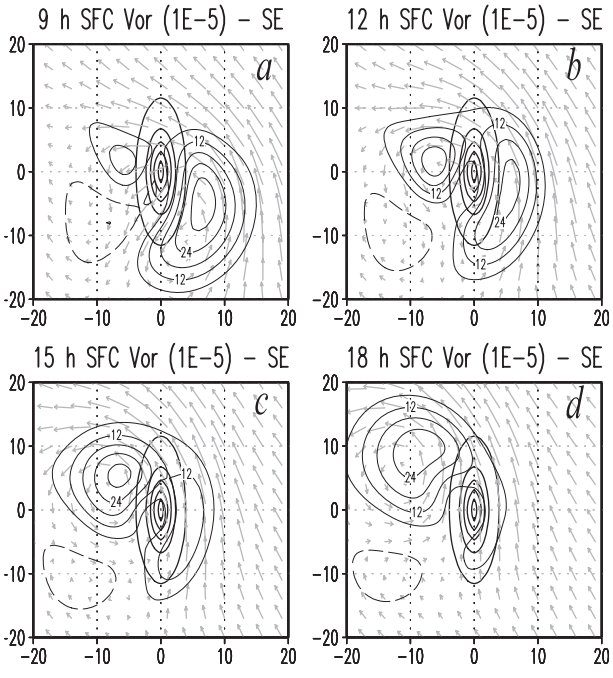

FIG. 12. As in Fig. 9, but for case SE.

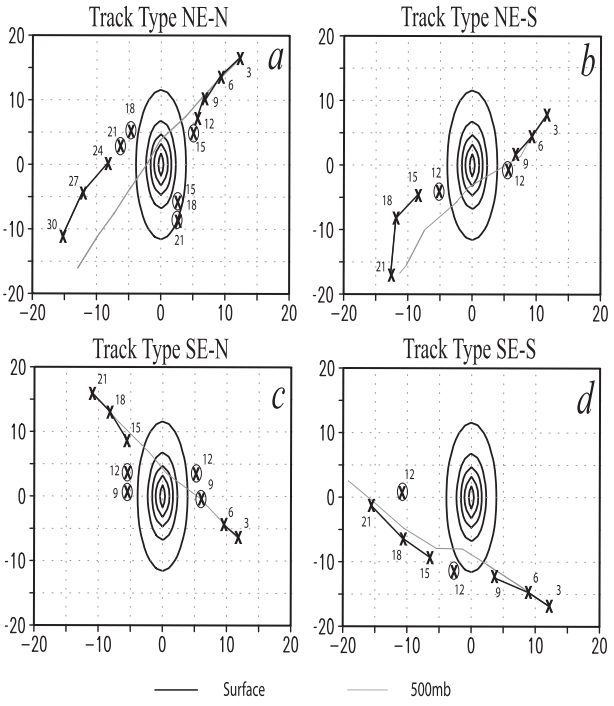

FIG. 13. GFDM simulated tracks of cyclone vortex centers from NE or SE landfalling on northern or southern mountain range—that is, track types (a) NE-N, (b) NE-S, (c) SE-N, and (d) SE-S—near the surface and at 500 mb. The crosses denote 3-hourly surface positions. A circled cross denotes a second, coexisting vortex center. Thick ovals denote terrain at every 400 m. Area shown is 800 km × 800 km.

center is dominated by vorticity stretching. At $t = 15$ h, the western center of positive vorticity is weakened by a strong negative vorticity advection, while the southern center remains deflected to the left, but is now influenced by vorticity stretching. At $t = 21$ h, the cyclone center resumes its northwestward movement, which is controlled by vorticity advection.

One example of track type SE-S is Typhoon Lorna (1961) (Fig. 1a), but its track is different from the ideally simulated track (Fig. 13d). This inconsistency might be due to a weaker blocking experienced by Typhoon Lorna, which produced a continuous track. Other examples of track type SE-S are Guilda (1956), Andy (1982), and Dot (1982) (Digital Typhoon 2011; Shieh et al. 1998).

4. Concluding remarks

In this study, the orographic effects of landfall location, approach angle, and their combination on track deflection during the passage of a cyclone vortex over a mesoscale mountain range are investigated using idealized modeling simulations. Conceptually, the track deflection can be explained by the degree of orographic blocking, measured by the Froude numbers associated with the basic wind U/Nh and the maximum wind of the cyclone vortex V_{max}/Nh (Lin et al. 2005).

For cyclone vortex landfall on the east-central part of the mountain (case E, track type E; Figs. 2a and 5), the surface cyclone is deflected slightly to the north before it encounters the mountain due to vorticity advection, slightly to the south as it is crossing over the mountain, and to the north after crosses the mountain due to stretching; then it resumes its original westward track far downstream (to the west) of the mountain due to vorticity advection. The surface cyclone vortex may turn to the south before encountering the mountain for strong blocking cases. For the cyclone vortex landfall in the northern part of the mountain from the east (case N, track type N; Figs. 2b and 9), the track is deflected in a way similar to that of track type E. For the cyclone vortex landfall in southern CMR from the east (case S, track type S; Figs. 2c and 10), the vortex center curves clockwise around the southern part of the mountain range owing to vorticity advection, overshoots to the north on the lee side as it is dominated by vorticity stretching, and then resumes westward movement far downstream because of vorticity advection.

For cyclone landfall at the east-central part of the mountain range from the northeast (track type NE; Figs. 2d and 11), its vortex center deviates slightly to the south due to vorticity advection associated with the northerly jet along the eastern flank of the mountain range. Note that the northerly jet used by Lin et al. (1999) and Jian and Wu (2008) to explain the southerly deflection, or looping, of typhoons over Taiwan's CMR is associated with flow splitting under strong orographic blocking (Fig. 4c; Lin et al. 2005). The cyclone vortex deviates to the right after passing the peak of the mountain range owing to vorticity stretching associated with flow splitting at the east-central landfall location. The vortex center then turns cyclonically and resumes southwestward movement far downstream due to vorticity advection. For cyclone landfall from the southeast (track type SE; Figs. 2e and 12), the track deflection of the surface cyclone is similar to track type E.

For a cyclone landfalling in northern CMR from the NE (track type NE-N, Fig. 13a), its vortex center is deflected to the left because of vorticity stretching. During its passage over the mountain, the lee side vorticity stretching becomes dominant, creating a rightward deflection. After passing over the mountain, vorticity advection controls the cyclone, which resumes its southwestward movement. For cyclone landfall at the southern part of the mountain range from the northeast (track type NE-S, Fig. 13b), the vortex center follows

a similar path to track type NE. For cyclone landfall at the northern part of the mountain range from the southeast (track type SE-N, Fig. 13c), the vortex center follows a similar path to track type SE. For cyclone landfall at the southern part of the mountain range from the southeast (track type SE-S, Fig. 13d), the vortex track is similar to track type SE except the vortex center is deflected to the left by a strong region of vorticity advection.

In summary, the deflection of a cyclone vortex encountering a mesoscale mountain range is largely controlled by vorticity advection and stretching, depending on the landfall location and approach angle of the cyclone. Specifically, for an elongated mesoscale mountain range, the local vorticity generation is more dominated by vorticity advection upstream of the mountain range, by vorticity stretching over the lee side and its immediate downstream area, and by vorticity advection again far downstream of the mountain as it steers the vortex back to its original direction of movement. The vorticity advection upstream of the mountain range is caused by flow splitting associated with orographic blocking. Note that the northerly jet used by Lin et al. (1999) and Jian and Wu (2008) to explain track type E or SE upstream southward deflection, or looping, of typhoons impinging on CMR is associated with this flow splitting under strong orographic blocking (Fig. 4c), as explained in Lin et al. (2005). The ideally simulated cyclone vortex tracks compare reasonably well with observed tracks of typhoons over Taiwan's CMR.

In analyzing the relative vorticity budget, we found that the jumps in vortex track are largely governed by stretching on the lee side of the mountain. Based on the vorticity equation, this stretching occurs where fluid columns descend the lee slope so that the rate of stretching is governed mostly by the flow speed and the terrain slope steepness. In other words, the maximum stretching and associated track jump are located on the faster side of the vortex. In the E and N cases, the faster winds are well north of the mountain crest, and the vortex track has very little change across the mountain. However, for the S case the stronger winds are near the center of the ridge, and the track jump is much larger. For the NE case, the jump in the vortex track occurs once the vortex center shifts south of the ridge. For the SE case, there is significant stretching, but it is aligned with the original motion of the vortex, so there is no jump in track.

This study may be extended to vary some major control parameters, such as U/Nh, $V_{\max}/Nh$, and R/L_y, to compare with typhoon tracks with real cases, to test the results with TC tracks over other mountain ranges, and to include moisture. Based on the dynamics found in this study, it is possible to factor the effects of landfall location and approach angle into the major control parameters proposed in Lin et al. (2005). For example, the effect of angle of approach α can be factored into the control parameter U/Nh by taking the component perpendicular to the mountain range as $U(\sin\alpha)/Nh$. The landfall location of the cyclone vortex may be factored into L_y in R/L_y. In addition, the Smith and Smith (1995) findings on PV generation over mountains might play an important role in changing the track and structure of the vortex downstream, although it is not clearly shown in the current results. The reasons might be twofold: (i) a more large-scale flow in the current case compared to the nonrotating fluid flow in the Smith and Smith study and (ii) the different behavior of a continuously stratified fluid flow in the current case. This is an important problem remained to be explored in the future but is beyond the current study.

Acknowledgments. The authors thank the help from C. M. Hill in the early stage of this study and S.-T. Wang for valuable discussions. This research is supported by the NOAA Educational Partnership Program (EPP) under Cooperative Agreement NA06OAR4810187.

REFERENCES

Bender, M. A., R. E. Tuleya, and Y. Kurihara, 1987: A numerical study of the effect of an island terrain on tropical cyclones. *Mon. Wea. Rev.,* **115,** 130–155.

Chang, S.W.-J., 1982: The orographic effects induced by an island mountain range on propagating tropical cyclones. *Mon. Wea. Rev.,* **110,** 1255–1270.

Clark, T. L., 1977: A small-scale dynamic model using a terrain following coordinate transformation. *J. Comput. Phys.,* **24,** 186–215.

Digital Typhoon, cited 2011: Typhoon images and information. National Institute of Informatics. [Available online at http://agora.ex.nii.ac.jp/digital-typhoon/index.html.en.]

Gary, J. M., 1973: Estimate of truncation error in transformed coordinate, primitive equation atmospheric models. *J. Atmos. Sci.,* **30,** 223–233.

Huang, C.-Y., and Y.-L. Lin, 1997: The evolution of a mesoscale vortex impinging on symmetric topography. *Proc. Natl. Sci. Counc. (Taiwan),* **21A,** 285–309.

Jian, G.-J., and C.-C. Wu, 2008: A numerical study of the track deflection of Supertyphoon Haitang (2005) prior to its landfall in Taiwan. *Mon. Wea. Rev.,* **136,** 598–615.

Lin, Y.-L., 2007: *Mesoscale Dynamics*. Cambridge University Press, 630 pp.

——, and T.-A. Wang, 1996: Flow regimes and transient dynamics of two-dimensional stratified flow over an isolated mountain ridge. *J. Atmos. Sci.,* **53,** 139–158.

——, J. Han, D. W. Hamilton, and C.-Y. Huang, 1999: Orographic influence on a drifting cyclone. *J. Atmos. Sci.,* **56,** 534–562.

——, S.-Y. Chen, C. M. Hill, and C.-Y. Huang, 2005: Control parameters for the influence of a mesoscale mountain range on

cyclone track continuity and deflections. *J. Atmos. Sci.,* **62,** 1849–1866.

O'Handley, C., and L. F. Bosart, 1996: The impact of the Appalachian Mountains on cyclonic weather systems. Part I: A climatology. *Mon. Wea. Rev.,* **124,** 1353–1373.

Schwierz, C. B., and H. C. Davies, 2003: Evolution of a synoptic-scale vortex advecting toward a high mountain. *Tellus,* **55A,** 158–172.

Shen, B.-W., and Y.-L. Lin, 1999: Effects of critical levels on two-dimensional back-sheared flow over an isolated mountain ridge on an *f* plane. *J. Atmos. Sci.,* **56,** 3286–3302.

Shieh, S.-L., S.-T. Wang, M.-D. Chen, and T.-C. Yeh, 1998: *Tropical Cyclone Tracks over Taiwan from 1897 to 1996 and Their Applications* (in Chinese). Central Weather Bureau, 497 pp.

Smith, R. B., and D. F. Smith, 1995: Pseudoinviscid wake formation by mountains in shallow-water flow with a drifting vortex. *J. Atmos. Sci.,* **52,** 436–454.

Wang, S.-T., 1980: Prediction of the movement and strength of typhoons in Taiwan and its vicinity. National Science Council (Taipei) Research Rep. 108, 100 pp.

Wang, T.-A., and Y.-L. Lin, 1999: Wave ducting in a stratified shear flow over a two-dimensional mountain. Part I: General linear criteria. *J. Atmos. Sci.,* **56,** 412–436.

Yeh, T.-C., and R. L. Elsberry, 1993a: Interaction of typhoons with the Taiwan topography. Part I: Upstream track deflections. *Mon. Wea. Rev.,* **121,** 3193–3212.

——, and ——, 1993b: Interaction of typhoons with the Taiwan topography. Part II: Continuous and discontinuous tracks across the island. *Mon. Wea. Rev.,* **121,** 3213–3233.

Zehnder, J. A., 1993: The influence of large-scale topography on barotropic vortex motion. *J. Atmos. Sci.,* **50,** 2519–2532.

——, and M. J. Reeder, 1997: A numerical study of barotropic vortex motion near a large-scale mountain range with application to the motion of tropical cyclones approaching the Sierra Madre. *Meteor. Atmos. Phys.,* **64,** 1–19.